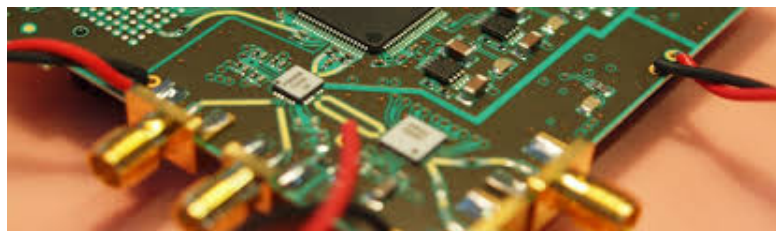


# A Terabit sampling system with a photonics time-stretch ADC

Master Thesis  
of

Olena Manzhura

at the Institute for Data Processing and Electronics (IPE)



Reviewer: Prof. Dr. Anke-Susanne Müller (LAS)  
Second Reviewer: Dr. Michele Caselle (IPE)

15.11.2020 – 13.08.2021



# Declaration

I hereby declare that I wrote my master thesis on my own and that I have followed the regulations relating to good scientific practice of the Karlsruhe Institute of Technology (KIT) in its latest form. I did not use any unacknowledged sources or means, and I marked all references I used literally or by content.

Karlsruhe, 13.08.2021, \_\_\_\_\_  
Olena Manzhura

Approved as an exam copy by

Karlsruhe, 13.08.2021, \_\_\_\_\_  
Prof. Dr. Anke-Susanne Müller (LAS)



# **Abstract**



# Zusammenfassung



# Résumé



# Contents

<b>1. Introduction</b>	<b>1</b>
<b>2. Theoretical Fundamentals</b>	<b>3</b>
2.1. Coherent Synchrotron Radiation . . . . .	3
2.1.1. Micro-Bunching Instability . . . . .	4
2.2. Photonic time-stretch analog-to-digital converter . . . . .	5
2.3. Characteristics of Analog-To-Digital-Converters . . . . .	6
2.3.1. Sampling Theory . . . . .	6
2.3.2. AC errors . . . . .	6
2.3.3. Interleaving . . . . .	7
2.4. RF/Microwave Design Basics . . . . .	8
<b>3. Design of the system</b>	<b>9</b>
3.1. General architecture . . . . .	9
3.1.1. KAPTURE-2 . . . . .	9
3.1.2. THERESA . . . . .	11
3.1.2.1. Xilinx Zynq UltraScale+ RFSoC ZCU216 Evaluation Kit .	11
3.1.3. Requirements . . . . .	12
3.2. Design of the front-end card . . . . .	14
3.2.1. Sampling-Channel . . . . .	14
3.2.2. Clocking . . . . .	14
3.2.3. Power Supply . . . . .	15
3.3. PCB-Layout . . . . .	16
3.3.1. General Techniques/Strategies? . . . . .	16
3.3.2. Floor Planning . . . . .	16
3.3.3. Transmission lines . . . . .	16
3.3.4. Polaris . . . . .	18
3.4. Firmware . . . . .	19
3.4.1. Xilinx Designs . . . . .	19
3.4.2. SPI-firmware for components . . . . .	19
3.4.3. IPE-AXI IP block . . . . .	19
3.4.4. GUI . . . . .	19
<b>4. Characterization</b>	<b>21</b>
4.1. Evaluation of the ZCU216 Board . . . . .	21
4.1.1. Measurements with Xilinx XM655 add-on card . . . . .	21
4.2. Measurements with the IPE front-end card . . . . .	21
<b>5. Conclusions and Outlook</b>	<b>23</b>
<b>Appendix</b>	<b>25</b>
A. QuickStart Guide for Evaluation of ZCU216 Board . . . . .	25
B. 3D model of front-end card . . . . .	25



# List of Figures

2.1.	CSR [Rot18] . . . . .	3
2.2.	Electro-Magnetic spectrum . . . . .	3
2.3.	Facility [Rot18] . . . . .	4
2.4.	Micro-bunching [BBB <sup>+</sup> 19] . . . . .	4
2.5.	Electro-Optical Time-Stretch Technique [BBB <sup>+</sup> 19] . . . . .	5
3.1.	General schema of KAPTURE-2 (cf. [CAB <sup>+</sup> 17, p.2]) . . . . .	9
3.2.	Signal with sample points . . . . .	10
3.3.	Photo of KAPTURE with highlighted main components. [Bro20, p. 61] . .	10
3.4.	General schema of THERESA. For presentation purposes only four channels are shown. . . . .	11
3.5.	ZCU216 evaluation board . . . . .	12
3.6.	RFSoC block diagram . . . . .	12
3.7.	Track-And-Hold Timing diagram . . . . .	13
3.8.	CLK104 Add-on board clocking scheme . . . . .	14
3.9.	Clocking scheme on front-end card . . . . .	15
3.10.	Edge-Coupled Coplanar Waveguide . . . . .	16
3.11.	Coplanar Waveguide with Ground . . . . .	17
3.12.	Polaris Solver . . . . .	18
3.13.	Test Graph . . . . .	18
4.1.	RF DC Evaluation Tool architecture [Xil20a] . . . . .	21
4.2.	RF DC Evaluation Tool GUI [Xil20a] . . . . .	21



## **List of Tables**

3.1. Power consumption of components on the board . . . . .	15
---	----



# List of abbreviations

<b>KIT</b>	Karlsruhe Institute of Technology
<b>IPE</b>	Institut für Prozessdatenverarbeitung und Elektronik
<b>KARA</b>	Karlsruhe Research Accelerator
<b>KAPTURE</b>	Karlsruhe Pulse Taking Ultra-fast Readout Electronics
<b>ADC</b>	Analog-To-Digital-Converter
<b>TAH</b>	Track-And-Hold
<b>PLL</b>	Phase-Locked-Loop
<b>FMC</b>	FPGA Mezzanine Card
<b>LVCMOS</b>	Low voltage complementary metal oxide semiconductor
<b>LVDS</b>	Low-voltage differential signaling
<b>LVPECL</b>	Low-voltage positive emitter-coupled logic
<b>PCIe</b>	PCI Express
<b>THERESA</b>	Terahertz Readout Sampling
<b>RFSoC</b>	Radio-Frequency System-On-Chip

# 1. Introduction

The ULTRASYNC (Exploration et contrôle ULTRArapide de la dynamique des paquets d'électrons dans les sources de lumière SYNChrotron, ANG-DFG) aims to study and control coherent synchrotron radiation (CSR) and microbunching instability. The goal is to obtain a high power and stable coherent emission (KARA and SOLEIL) by feedback control. At SOLEIL, this was already successfully achieved, still there is a significant limit to the range, where this concept works. One possible way would be to calculate the necessary feedback from a whole THz CSR pulse shape, which would require to record an electro-optical signal (time-stretch). This leads to a possible approach by combining time-stretch and FPGA.

For the moment, the only experimental test has been made using a relatively simple feedback: - a bolometer signal as the feedback loop input - a low-cost FPGA (redpitaya) that sends the feedback on the accelerating voltage There are limitations in the maximal bunch charge in the accelerator. So an open question is whether measuring each THz pulse using EO sampling + time-stretch may help to solve this open problem. In clear: - EO sampling + time-stretch as in Eléonore's thesis -> association with the new FPGA-based system -> finding adequate feedback that is programmed in the FPGA may solve the problem, and allow the control to succeed at the highest currents in SOLEIL. Target would be 15 mA for 1 bunch (and feedback control presently works to a little more than 10 mA).

At 1 micron wavelength, the maximum stretch is limited due to fiber glass properties (at this wavelength). The maximum length achieved are 2-4 ns (SOLEIL and KARA). For this reason, a fast ADC is critical, to get a good ENOB/number of sampling points. A relevant figure of merit (that characterizes the effective number of points) is – we think: FOM=electronic bandwidth x stretch time. There is some bottleneck concerning time-stretch at this wavelength, and one way to solve the issue is to try pushing the bandwidth of ADCs.

At 1550 nm wavelength, it is possible to stretch the signal up to tens of nanoseconds. Therefore, a relatively cheap ADC would already be sufficient and allow an effective number of samples at around 100. Applications still need to be investigated.

As potential applications for the new system would be applications for accelerators in the 1 micron wavelength (best concerning EO sampling SNR and bandwidth).



## 2. Theoretical Fundamentals

### 2.1. Coherent Synchrotron Radiation

Relativistic electron bunches circulating in storage rings are used to produce intense radiation from far-infrared to X-rays. However, above a density threshold value, the interaction between the electron bunch and its own radiation can lead to a spatio-temporal instability called microbunching instability. This instability is characterized by a strong emission of coherent THz radiation (typically 100000 times stronger than the classical synchrotron radiation) which is a signature of the presence of microstructures (at mm scale) in the electron bunch. This instability is known to be a fundamental limitation of the operation of synchrotron light sources at high beam current.

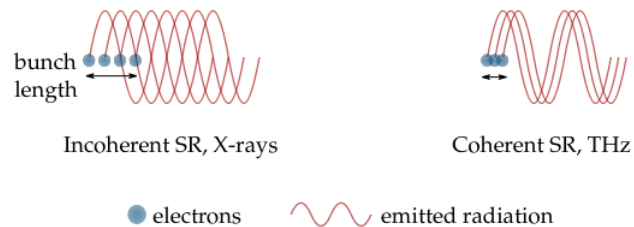


**Figure 2.1.:** CSR [Rot18]

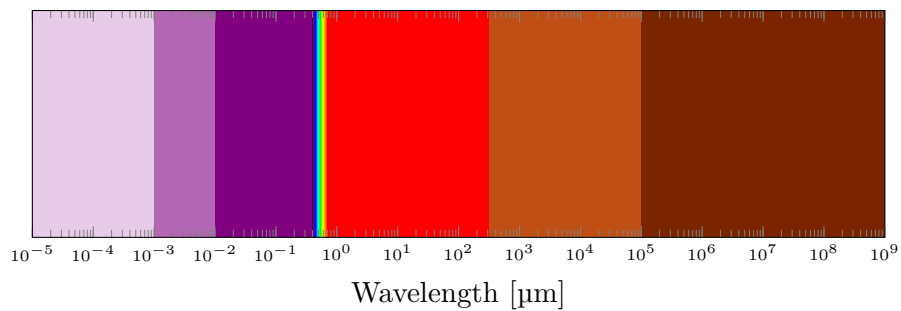


**Figure 2.2.:** Electro-Magnetic spectrum

## KARA

- Located at the Karlsruhe Institute of Technology (KIT)
- Up to 184 electron packages (bunches) can be filled with a distance between two adjacent bunches of 2 ns
- Operated by the Institute of Beam Physics and Technology (IBPT)

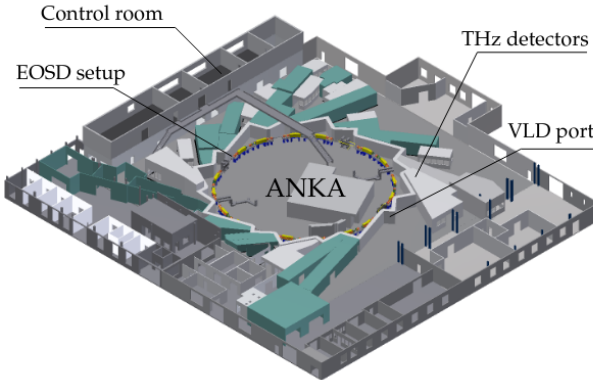


**Figure 2.3.:** Facility [Rot18]

### 2.1.1. Micro-Bunching Instability

in the quest for higher emitted synchrotron radiation power, electron bunches with high charge densities are naturally subject to a complex nonlinear dynamics which can lead to instabilities. The so-called microbunching instability or CSR (Coherent Synchrotron Radiation) instability (due to the interaction of the electrons with their own radiation in bending magnets) is known to be responsible for the spontaneous formation of microstructures in the bunch. This spatio-temporal instability is recognized to be a fundamental limitation of stable operation at high current density in storage rings. In parallel, it is also considered as a promising source of brilliant THz radiation at high repetition rate.

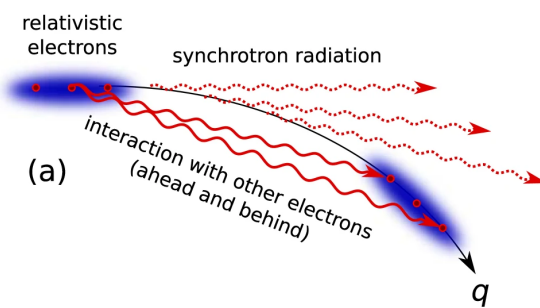


**Figure 2.4.:** Micro-bunching [BBB<sup>+</sup>19]

## 2.2. Photonic time-stretch analog-to-digital converter

" In recent and future synchrotron radiation facilities, relativistic electron bunches with increasingly high charge density are needed for producing brilliant light at various wavelengths, from X-rays to terahertz. In such conditions, interaction of electron bunches with their own emitted electromagnetic fields leads to instabilities and spontaneous formation of complex spatial structures. Understanding these instabilities is therefore key in most electron accelerators. However, investigations suffer from the lack of non-destructive recording tools for electron bunch shapes. In storage rings, most studies thus focus on the resulting emitted radiation. Here, we present measurements of the electric field in the immediate vicinity of the electron bunch in a storage ring, over many turns. For recording the ultrafast electric field, we designed a photonic time-stretch analog-to-digital converter with terasamples/second acquisition rate. We could thus observe the predicted link between spontaneous pattern formation and giant bursts of coherent synchrotron radiation in a storage ring. "' [BBB<sup>+</sup>19]

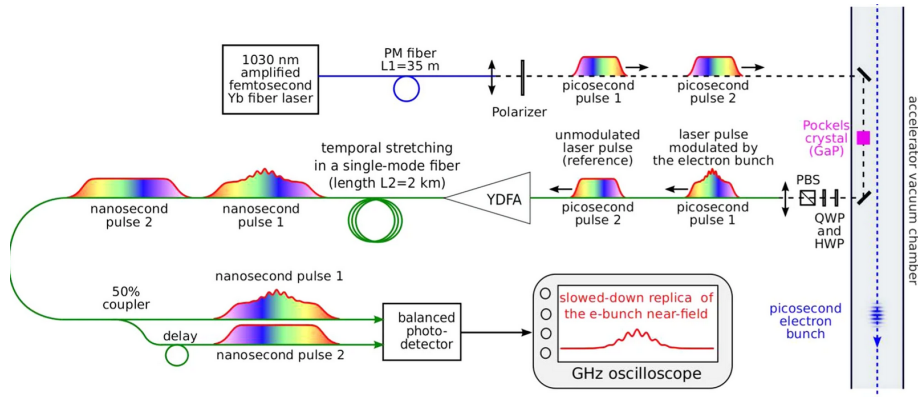


**Figure 2.5.:** Electro-Optical Time-Stretch Technique [BBB<sup>+</sup>19]

## 2.3. Characteristics of Analog-To-Digital-Converters

Analog-to-digital converters (ADCs) are used to translate analog quantities into digital signals, which can be processed by information processing, computing, data transmission and control systems. This section covers the different characteristics of an ADC, which are needed to evaluate the performance of the developed system.

### 2.3.1. Sampling Theory

#### Nyquist-Criteria

An ADC samples an analog signal with a frequency  $f_s$ . This frequency has to be chosen in such way, that the original signal can be fully reconstructed. The Nyquist criteria states, that in order to accurately represent a bandlimited, continuous signal

$$y(t) \circlearrowleft Y(f) \quad \text{with} \quad Y(f) = 0, |f| \geq \frac{B}{2} \quad (2.1)$$

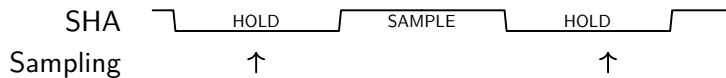
it has to be sampled with a frequency  $f_s$  respecting

$$f_s \geq B \quad \text{or} \quad f_s \geq 2f_a \quad (2.2)$$

with  $f_a$  being the highest frequency contained in the signal. [Kes05] [Pue15]

#### Sample-And-Hold-Amplifier

ADCs need a certain amount of time to sample the input signal. If the value of the signal changes by more than one Least-Significant-Bit (LSB) during this period, this can result in large errors in the output signal. Therefore, so called Sample-And-Hold-Amplifiers (SHA) are used in front of ADCs to hold the input value for the needed amount of time. The ADC sampling needs to be timed in such way, that the analog-to-digital conversion falls into the hold period of the SHA and doesn't exceed into the sample period.



### 2.3.2. AC errors

- Quantization Noise
- Equivalent Input Referred Noise
- Noise-Free Code Resolution

#### Integral and Differential Nonlinearity Distortion

#### Dynamic Performance

- Harmonic Distortion, Worst Harmonic, Total Harmonic Distortion (THD), Total Harmonic Distortion + Noise (THD + N)
- Signal-to-Noise-and-Distortion Ratio (SINAD, or S/N + D), Signal-to-Noise ratio (SNR), Effective Number of Bits (ENOB)
- Analog Bandwidth (Full-Power, Small-Signal)
- Spurious Free Dynamic Range (SFDR)

- Two-Tone Intermodulation Distortion, Multi-Tone Intermodulation Distortion
- Noise Power Ratio (NPR)
- Adjacent Leakage Ratio (ACLR)
- Noise Figure
- Setting Time, Overvoltage Recovery Time

[Kes05]

### **2.3.3. Interleaving**

- Net sample rate
- Interleaving Spurs

[MR15]

## 2.4. RF/Microwave Design Basics

### 3. Design of the system

This chapter covers the architecture and design of the system.

#### 3.1. General architecture

In this section the general architecture of the THERESA system is described. The idea for the new system is to reuse the concept of the already existing sampling system KAPTURE (**K**arlsruhe **P**ulse **T**aking **U**ltra-fast **R**eadout **E**lectronics), which is using four ADCs, and expanding it to 16. Therefore, also the architecture of the latter is explained briefly.

##### 3.1.1. KAPTURE-2

KAPTURE, which was developed at IPE, is a system designed to continuously sample ultra-short pulses generated by Terahertz detectors. It consists of a daughter card, holding four sampling channels, mounted on a FPGA . The FPGA is connected to a computer via PCIe for further processing of the acquired data. [Bro20] The newer version, KAPTURE-2, was designed for more accurate sampling for pulse repetition rates up to 2 GHz. The acquired data is processed with a FPGA and GPU architecture. [CAB<sup>+</sup>17]

The general structure of the board is shown in Figure 3.3.

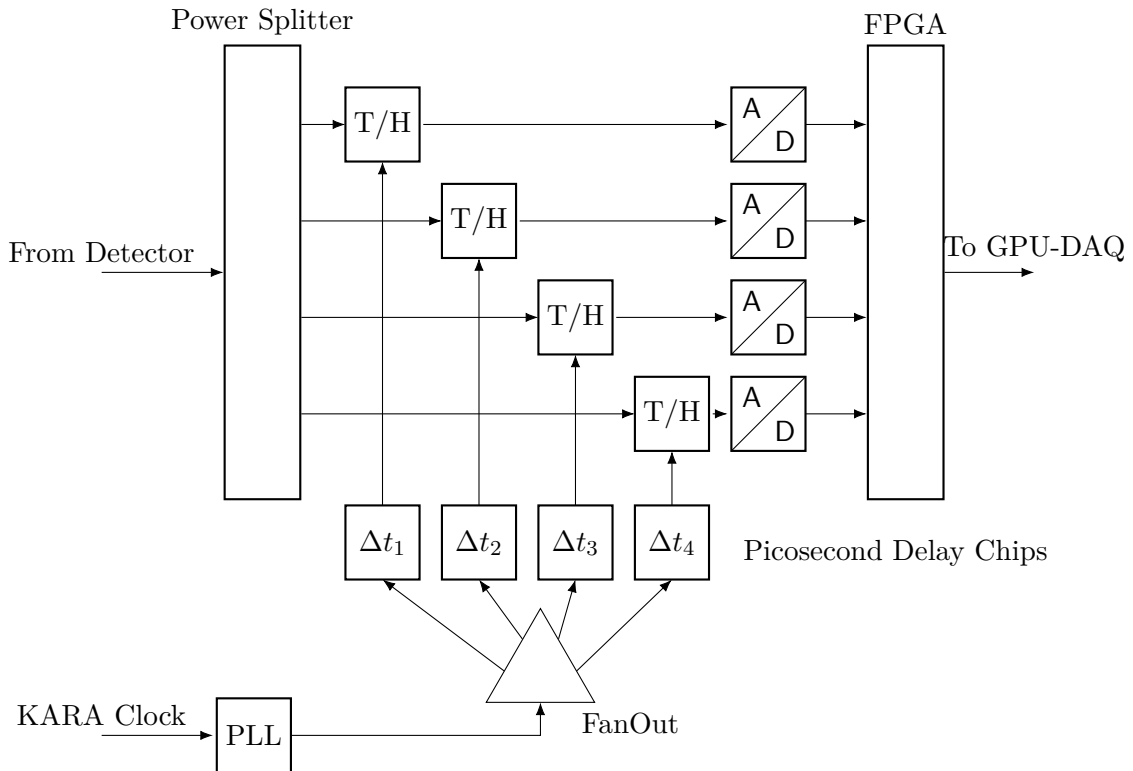


**Figure 3.1.:** General schema of KAPTURE-2 (cf. [CAB<sup>+</sup>17, p.2])

The pulse from the THz detector is fed into a power splitter, which splits the signal into four identical pulses and distributes them to four channels, consisting of a respective Track-And-Hold-Amplifier (THA) unit and a 12-bit ADC@500 MS/s. The sampling time of each unit can be adjusted individually with a Picosecond Delay Chip with a resolution of 3 ps (maximal delay range: 100 ps). The clock signal is provided by KARA, which cleared from jitter by a Phase-Locked-Loop (PLL). This ensures the synchronization of the ADCs with the RF system. The clean clock signal is distributed to the delay chips via fan-out. [CAB<sup>+17]</sup>

The resulting sampling of the detector signal is shown Figure 3.2 (simplified representation).

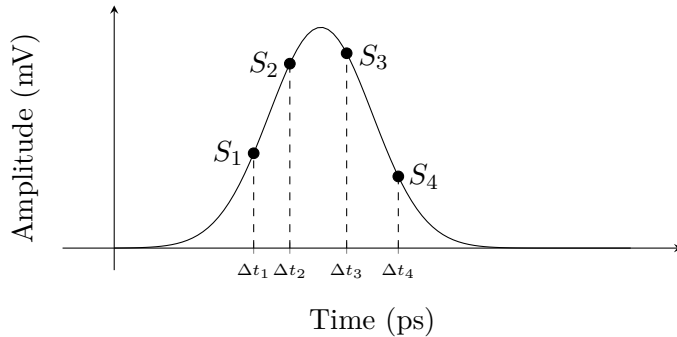


**Figure 3.2.:** Signal with sample points

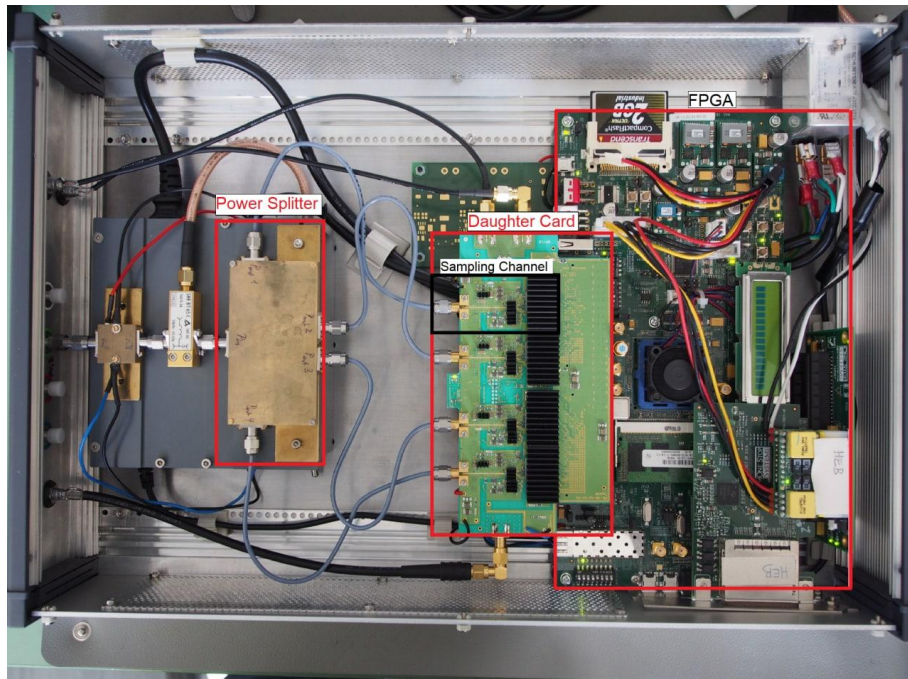


**Figure 3.3.:** Photo of KAPTURE with highlighted main components. [Bro20, p. 61]

### 3.1.2. THERESA

In principle, the new system has the same structure, as KAPTURE. Notable differences are firstly the number of ADCs, which is increased up to 16. Secondly, the latter are not located on the daughter card anymore, but inside the Xilinx Zynq UltraScale+ RFSoC ZU49DR on the ZCU216 Evaluation Kit on which the front-end card is mounted. Figure 3.4 shows the general schema of the sampling system, reduced to four channels for presentation purposes.

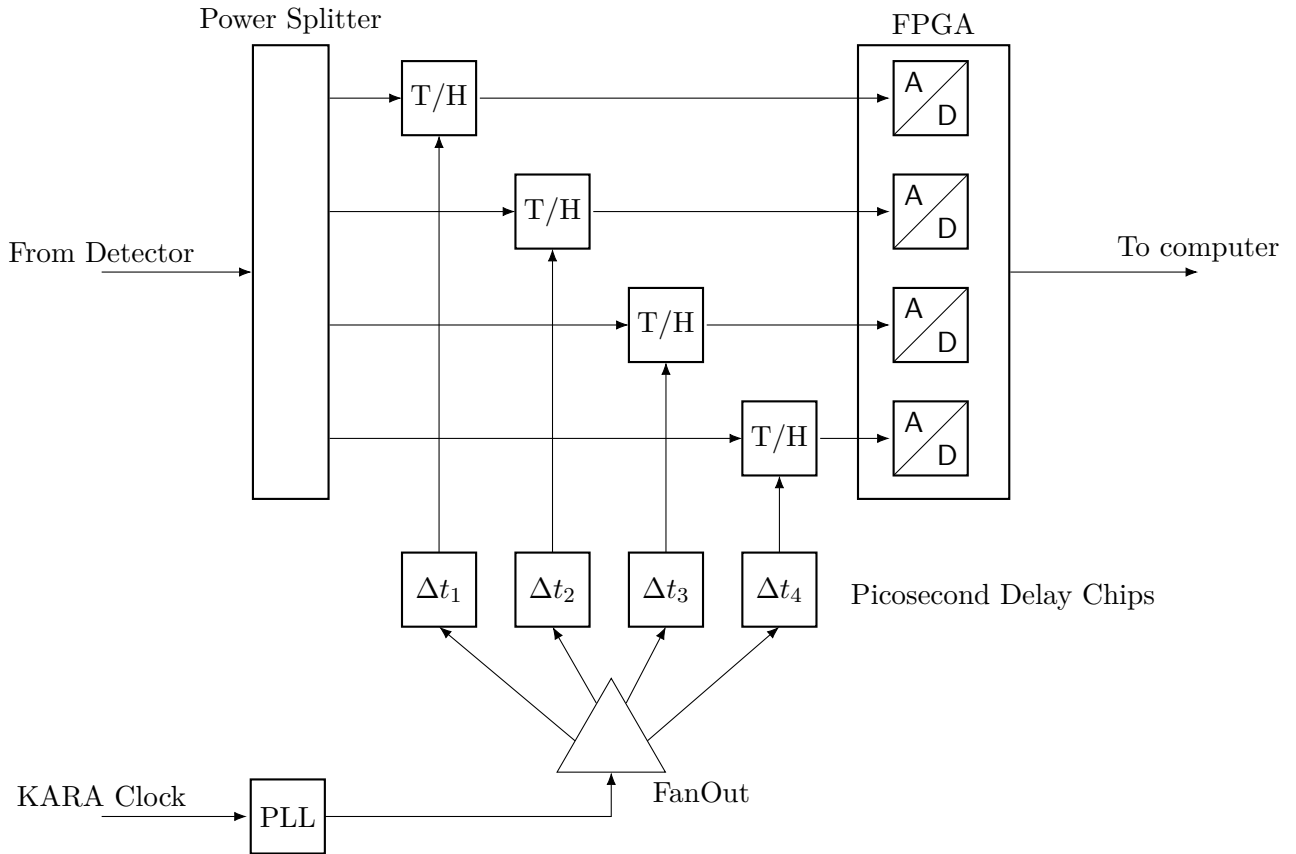
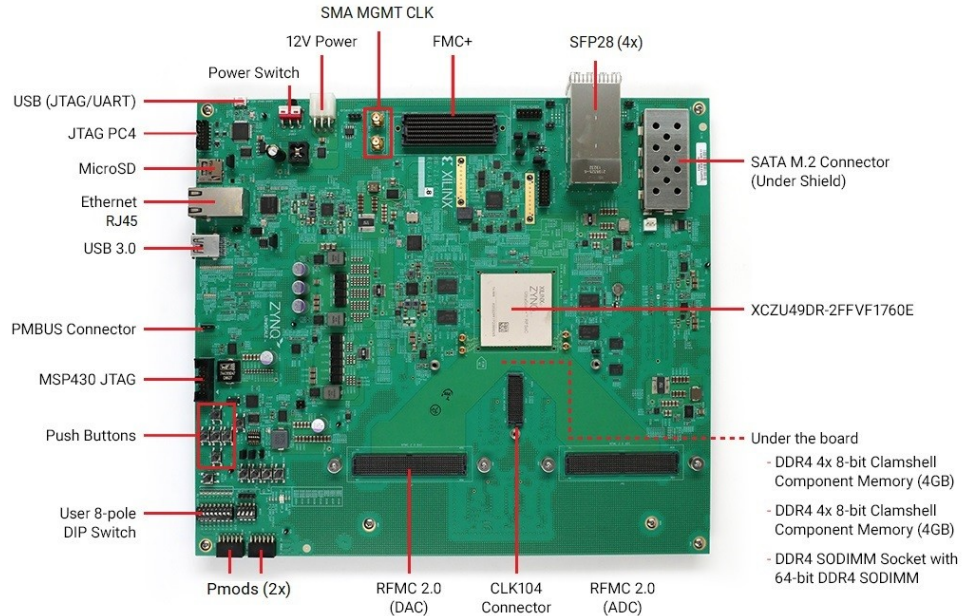


**Figure 3.4.:** General schema of THERESA. For presentation purposes only four channels are shown.

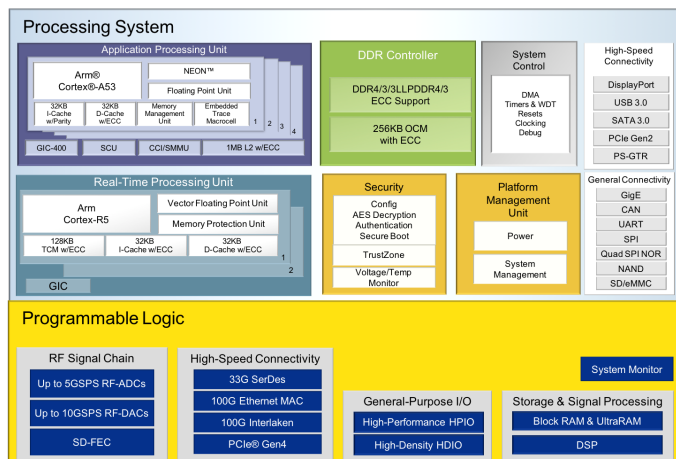
#### 3.1.2.1. Xilinx Zynq UltraScale+ RFSoC ZCU216 Evaluation Kit

The card, holding the sampling channels, should be mounted on a ZCU216 evaluation board. This board is the newest generation of Xilinx' evaluation cards, which has features suitable for the purpose at hand.

- Sixteen 14-bit, 2.5GSPS RF-ADC
- Sixteen 14-bit, 10GSPS RF-DAC
- I/O expansion options – FPGA Mezzanine Card (FMC+) interfaces, RFMC 2.0 interfaces, and Pmod connections



**Figure 3.5.:** ZCU216 evaluation board

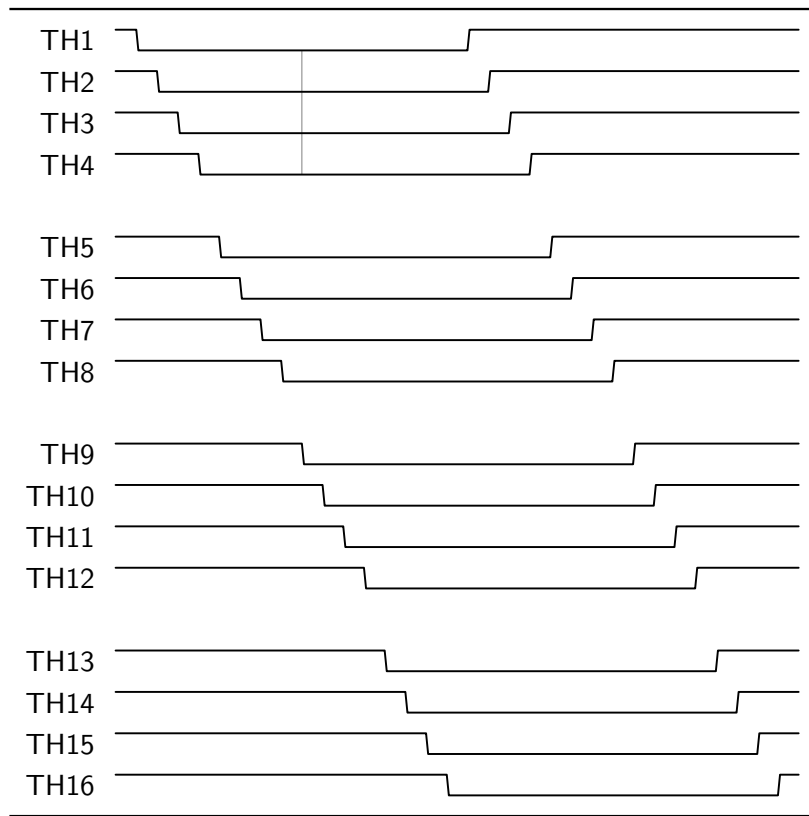


**Figure 3.6.:** RFSoC block diagram

### 3.1.3. Requirements

#### Step size delay chip

The necessary step size for the delay chips, when using 16 ADC@2 GS/s in time-interleaving mode, is:  $\frac{2 \text{ GS/s}}{16} = 31 \text{ ps}$

**Frequency****Figure 3.7.:** Track-And-Hold Timing diagram**Data Rate****Visualization/GUI**

### 3.2. Design of the front-end card

In this section, the design of the front-end card is covered.

### 3.2.1. Sampling-Channel

## Delay Chip NB6L295

Dual Channel Programmable Delay Chip.

- Two individual variable delay channels
  - Dual Delay: minimal delay 3.2 ns
  - Total Delay Range: 3.2 ns to 8.8 ns per Delay Channel
  - 11 ps Increments in 511 steps
  - 100 ps Typical Rise and Fall Times

### 3.2.2. Clocking

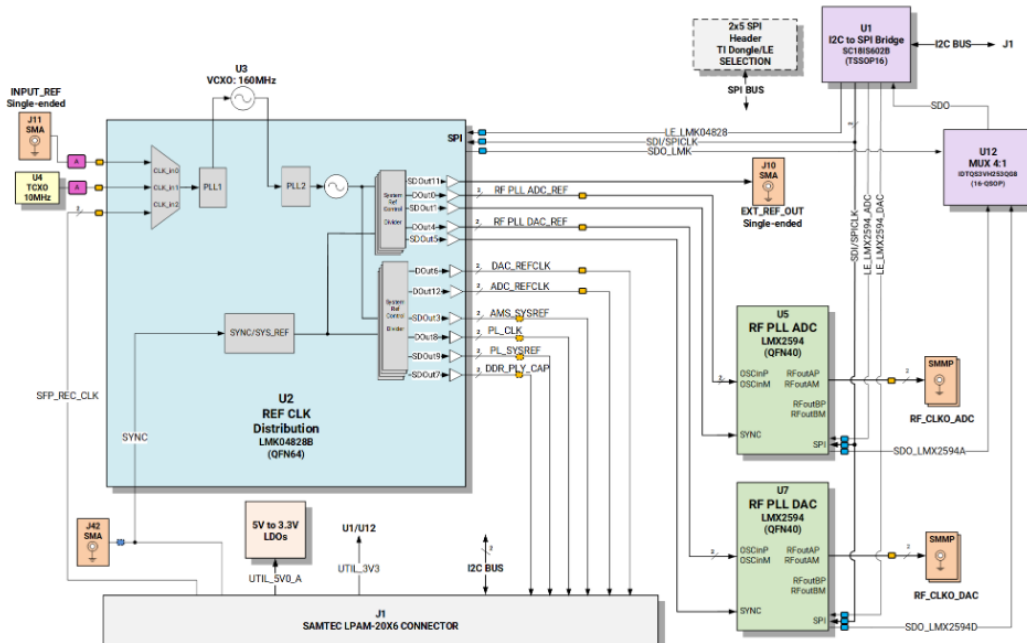


**Figure 3.8.:** CLK104 Add-on board clocking scheme

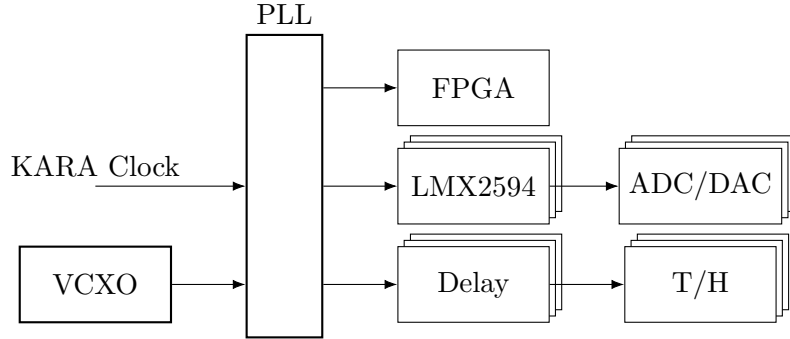


**Figure 3.9.:** Clocking scheme on front-end card

### 3.2.3. Power Supply

For the Track-And-Hold amplifiers a new power supply unit – the ADP1741 (Analog Devices) – should be used. It is necessary to think about the amount of power supply chips needed. As a rule of thumb, the power supply should provide twice the maximum power needed by the components it drives. The power consumption/maximum current for the respective components on the THERESA board is listed in Table 3.1.

**Table 3.1.:** Power consumption of components on the board

Component	$V_{cc}$ (V)	$I_{max}$ (A)	$P_{max}$ (W)	#parts	$I_{tot}^1$ (A)
HMC5649 (T/H-Amplifier)	2	0.221	0.442	16	3.536
	-5	-0.242	1.21		3.872
HMC856 (Delay)	-3.3	0.185	-0.611	16	2.96
HMC987LP5E (Fan-Out)	3.3	0.234 <sup>2</sup>	0.772	2	0.468
LMC0480 (PLL)	3.3	0.590 <sup>3</sup>	1.947	1	0.590
VCXO	3.3	0.03	0.198	1	0.03

<sup>1</sup>for 16 ADCs

<sup>2</sup>All Outputs and RF-Buffer

<sup>3</sup>All CLKs

The maximal current which the ADP1741 can provide @2 V is 2 A. This means, with one Track-And-Hold amplifier requiring a maximal current of 0.221 A, one ADP1741 can handle four units according to the rule mentioned beforehand ( $I_{max\_ADP1741} = 2 \text{ A} > 2 * I_{tot}, I_{tot} = 4 * 0.221 \text{ A} = 0.884 \text{ A}$ ).

### 3.3. PCB-Layout

#### 3.3.1. General Techniques/Strategies?

#### 3.3.2. Floor Planning

#### 3.3.3. Transmission lines

##### Surface Coplanar Waveguide with Ground

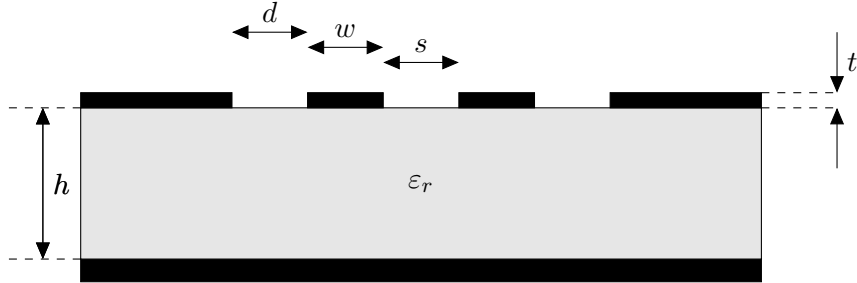


**Figure 3.10.:** Edge-Coupled Coplanar Waveguide

The corresponding equations are [Wad91, p197-198]:

$$Z_{0,o} = \frac{\eta_0}{\sqrt{\epsilon_{eff,o}}} \left( \frac{1.0}{2.0 \frac{K(k_o)}{K'(k_o)} + \frac{K(\beta_1)}{K'(\beta_1)}} \right) \quad (3.1)$$

$$Z_{0,e} = \frac{\eta_0}{\sqrt{\epsilon_{eff,e}}} \left( \frac{1.0}{2.0 \frac{K(k_e)}{K'(k_e)} + \frac{K(\beta_1 k_1)}{K'(\beta_1 k_1)}} \right) \quad (3.2)$$

$$\epsilon_{eff,o} = \frac{2.0 \epsilon_r \frac{K(k_o)}{K'(k_o)} + \frac{K(\beta_1)}{K'(\beta_1)}}{2.0 \frac{K(k_o)}{K'(k_o)} + \frac{K(\beta_1)}{K'(\beta_1)}} \quad (3.3)$$

$$\epsilon_{eff,e} = \frac{2.0 \epsilon_r \frac{K(k_e)}{K'(k_e)} + \frac{K(\beta_1 k_1)}{K'(\beta_1 k_1)}}{2.0 \frac{K(k_e)}{K'(k_e)} + \frac{K(\beta_1 k_1)}{K'(\beta_1 k_1)}} \quad (3.4)$$

Where

$$k_o = \Lambda \frac{-\sqrt{\Lambda^2 - t_c^2} + \sqrt{\Lambda^2 - t_B^2}}{t_B \sqrt{\Lambda^2 - t_c^2} + t_c \sqrt{\Lambda^2 - t_B^2}} \quad (3.5)$$

$$k_e = \Lambda' \frac{-\sqrt{\Lambda'^2 - t'_c^2} + \sqrt{\Lambda'^2 - t'_B^2}}{t'_B \sqrt{\Lambda'^2 - t'_c^2} + t'_c \sqrt{\Lambda'^2 - t'_B^2}} \quad (3.6)$$

$$\Lambda = \frac{\sinh^2 \left( \frac{\pi(s/2.0 + w + d)}{2.0h} \right)}{2} \quad (3.7)$$

$$t_c = \sinh^2 \left( \frac{\pi(s/2.0 + w)}{2.0h} \right) - \Lambda \quad (3.8)$$

$$t_B = \sinh^2 \left( \frac{\pi s}{4.0h} \right) - \Lambda \quad (3.9)$$

$$\Lambda' = \frac{\cosh^2 \left( \frac{\pi(s/2.0+w+d)}{2.0h} \right)}{2} \quad (3.10)$$

$$t'_c = \sinh^2 \left( \frac{\pi(s/2.0+w)}{2.0h} \right) - \Lambda' + 1.0 \quad (3.11)$$

$$t'_B = \sinh^2 \left( \frac{\pi s}{4.0h} \right) - \Lambda + 1.0 \quad (3.12)$$

The parameters have to be chosen according to

$$s + 2.0w + 2.0d \leq h \quad (3.13)$$

to guarantee coplanar propagation. [Wad91]

### Surface Coplanar Waveguide with Ground

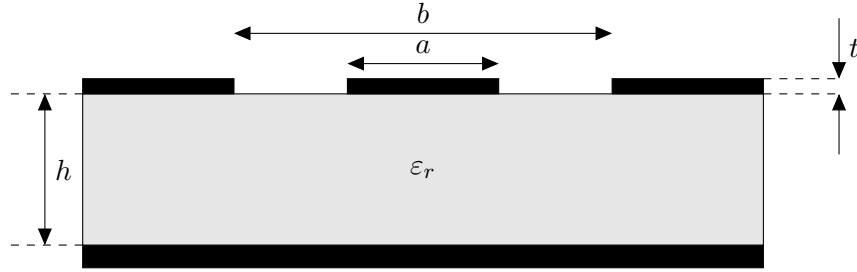


**Figure 3.11.:** Coplanar Waveguide with Ground

The characteristic impedance of a coplanar waveguide is given as follows [Wad91]:

$$Z_0 = \frac{60.0\pi}{\sqrt{\epsilon_{eff}}} \frac{1.0}{\frac{K(k)}{K(k')} + \frac{K(k_1)}{K(k'_1)}} \quad (3.14)$$

It comprises of the following components, with  $K(k)$  being an elliptical integral of the first kind (see also [BSMM99, p. 430]):

$$k = a/b \quad (3.15)$$

$$k' = \sqrt{1.0 - k^2} \quad (3.16)$$

$$k'_1 = \sqrt{1.0 - k_1^2} \quad (3.17)$$

$$k_1 = \frac{\tanh(\frac{\pi a}{4.0h})}{\tanh(\frac{\pi b}{4.0h})} \quad (3.18)$$

$$\epsilon_{eff} = \frac{1.0 + \epsilon_r \frac{K(k')}{K(k)} \frac{K(k_1)}{K(k'_1)}}{1.0 + \frac{K(k')}{K(k)} \frac{K(k_1)}{K(k'_1)}} \quad (3.19)$$

### 3.3.4. Polaris

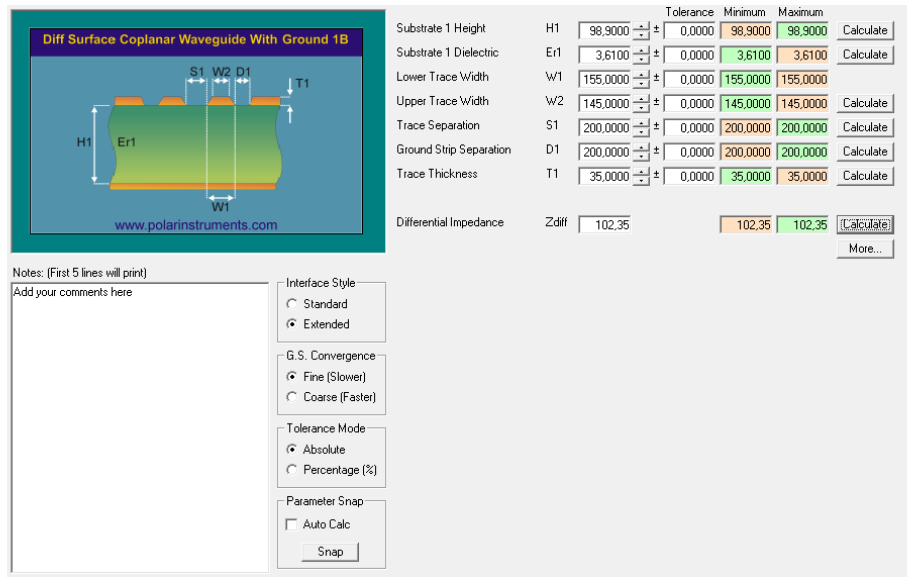


**Figure 3.12.:** Polaris Solver

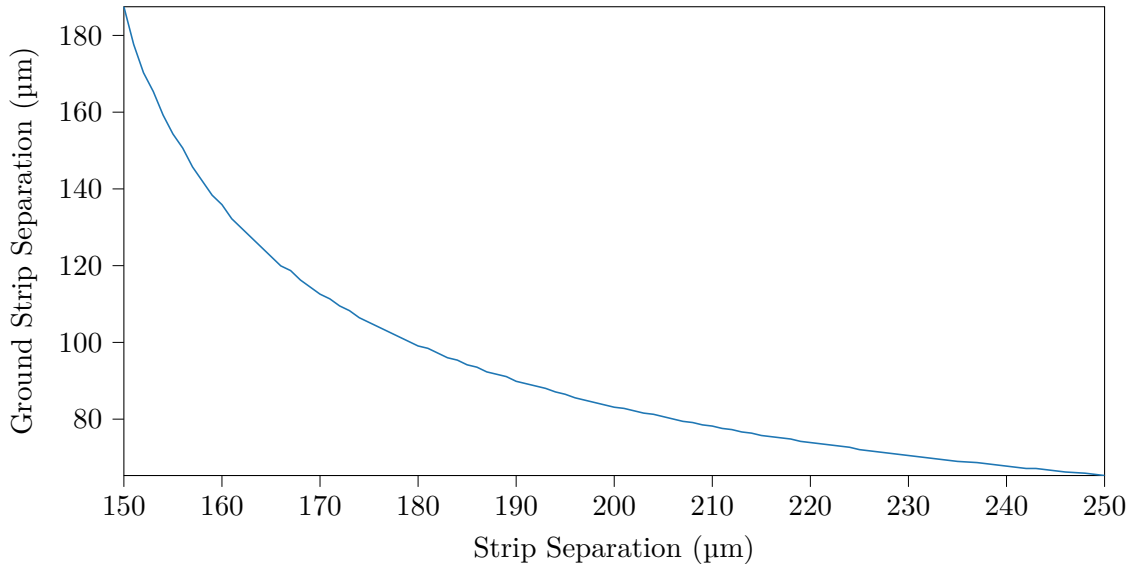


**Figure 3.13.:** Test Graph

### **3.4. Firmware**

#### **3.4.1. Xilinx Designs**

#### **3.4.2. SPI-firmware for components**

#### **3.4.3. IPE-AXI IP block**

#### **3.4.4. GUI**



# 4. Characterization

## 4.1. Evaluation of the ZCU216 Board

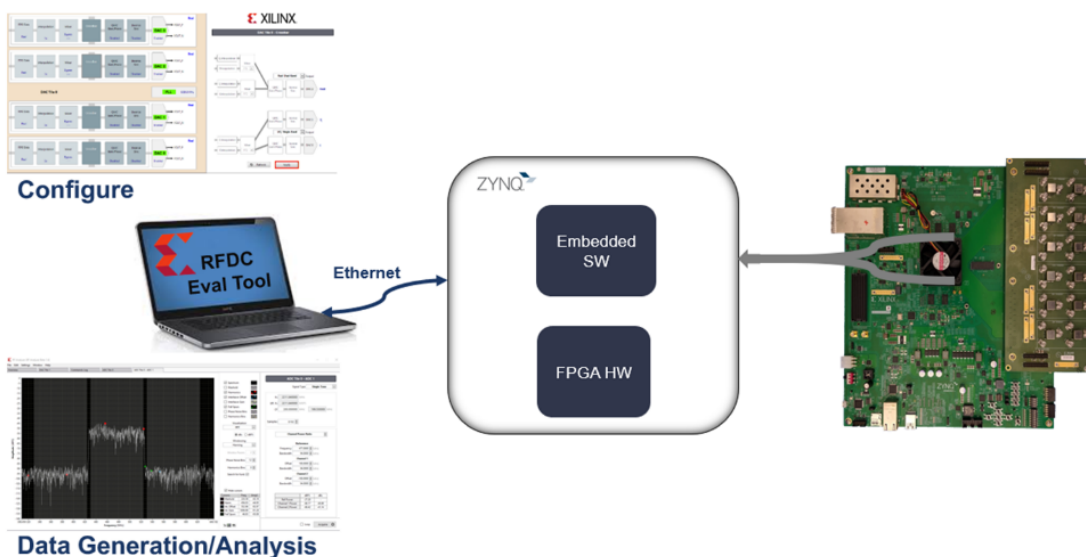


Figure 4.1.: RF DC Evaluation Tool architecture [Xil20a]

### 4.1.1. Measurements with Xilinx XM655 add-on card

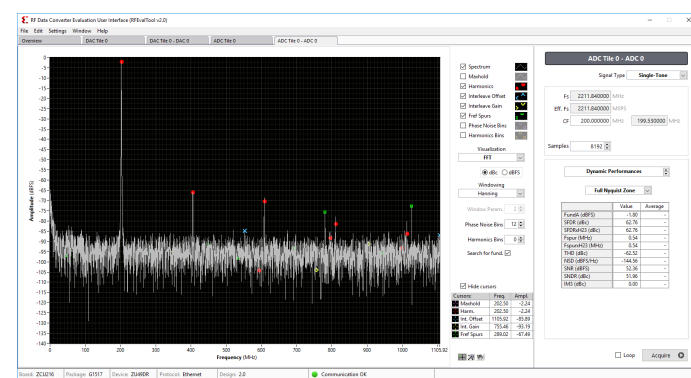


Figure 4.2.: RF DC Evaluation Tool GUI [Xil20a]

## 4.2. Measurements with the IPE front-end card



## **5. Conclusions and Outlook**



# Appendix

A. QuickStart Guide for Evaluation of ZCU216 Board

B. 3D model of front-end card



# Bibliography

- [BBB<sup>+</sup>19] Bielawski, Serge, Edmund Blomley, Miriam Brosi, Erik Bründermann, Eva Burkard, Clément Evain, Stefan Funkner, Nicole Hiller, Michael Nasse, Gundrun Niehues und et al.: *From self-organization in relativistic electron bunches to coherent synchrotron light: observation using a photonic time-stretch digitizer*. Scientific Reports, 9(1), July 2019. <http://dx.doi.org/10.1038/s41598-019-45024-2>.
- [Bro20] Brosi, Miriam: *In-Depth Analysis of the Micro-Bunching Characteristics in Single and Multi-Bunch Operation at KARA*. Dissertation, Karlsruher Institut für Technologie (KIT), 2020. 54.01.01; LK 01.
- [BSMM99] Bronstein, Semendjajew, Musiol und Mühlig: *Taschenbuch der Mathematik*. Verlag Harri Deutsch, 1999.
- [CAB<sup>+</sup>17] Caselle, M., L.E. Ardila Perez, M. Balzer, A. Kopmann, L. Rota, M. Weber, M. Brosi, J. Steinmann, E. Bründermann und A. S. Müller: *KAPTURE-2. A picosecond sampling system for individual THz pulses with high repetition rate*. Journal of Instrumentation, 12, 2017.
- [Kes05] Kester, Walt: *The Data Conversion Handbook*. Newnes, 2005.
- [MR15] Manganaro, Gabriele und Dave Robertson: *Interleaving ADCs: Unraveling the Mysteries*. Analog Dialogue, 2015.
- [Pue15] Puente León, Fernando: *Messtechnik - Systemtheorie für Ingenieure und Informatiker*. Vieweg Verlag, 10. aufl. Auflage, 2015, ISBN 978-3-662-44820-5.
- [Rot18] Rota, Lorenzo: *KALYPSO, a novel detector system for high-repetition rate and real-time beam diagnostics*. Dissertation, Karlsruher Institut für Technologie (KIT), 2018. 54.02.02; LK 01.
- [Wad91] Wadell, Brian C.: *Transmission Line Design Handbook*. Artech House, 1991.
- [Xil20a] Xilinx: *UG1433 - Zynq UltraScale+ RFSoCZCU208 and ZCU216 RFData Converter Evaluation Tool User Guide*. [https://www.xilinx.com/support/documentation/boards\\_and\\_kits/zcu216/ug1433-zcu216-rfsoc-eval-tool.pdf](https://www.xilinx.com/support/documentation/boards_and_kits/zcu216/ug1433-zcu216-rfsoc-eval-tool.pdf), June 2020.
- [Xil20b] Xilinx: *UG1437 - CLK104 RF Clock Add-onCard User Guide*. [https://www.xilinx.com/support/documentation/boards\\_and\\_kits/zcu216/ug1437-clk104.pdf](https://www.xilinx.com/support/documentation/boards_and_kits/zcu216/ug1437-clk104.pdf), March 2020.